Measurement and modelling of the high-power performance of carbon-based supercapacitors

Peter J. Mahon [a,*], George L. Paul [a], Sarkis M. Keshishian [a], Anthony M. Vassallo [b]

[a] *cap-XX Pty Ltd., Unit 9-10, 12 Mars Road, Lane Cove, NSW 2066, Australia*
[b] *CSIRO Energy Technology, North Ryde, NSW 2113 Australia*

Abstract

Supercapacitors are now being looked at for use in higher power applications such as mobile telecommunications and hybrid electric vehicles. We have examined two different supercapacitors, one is a commercial sample and the other is a supercapacitor of our own design. Four different testing methods including Impedance Spectroscopy, Constant Current Charging, Cyclic Voltammetry and Power Cycling were applied to each supercapacitor and the results are reviewed.

Parameter values obtained from Impedance Spectroscopy are excellent for comparing supercapacitors under equilibrium conditions but correlate poorly with data obtained from the more useful Power Cycling Charts (PCC). The choice of the current step size in Constant Current Charging and the scan rate in Cyclic Voltammetry has a large bearing on the results obtained from these techniques.

The strong voltage dependence of the parameters for the commercial sample prevented analysis using Cyclic Voltammetry. It was also clearly demonstrated by Power Cycling that the commercial sample had the poorer power performance of the two supercapacitors tested. It is concluded that for high-powered applications such as telecommunications and wireless protocols the most useful comparison of supercapacitor capability is through the PCC. © 2000 Elsevier Science S.A. All rights reserved.

Keywords: Supercapacitor; Power cycling; Constant current charging; Cyclic voltammetry; Impedance spectroscopy; Ragone plot

1. Introduction

Supercapacitors are now being used in a number of applications, mostly as low-power devices for the purpose of memory data backup [1–3]. It is expected that as supercapacitors move into other applications higher power densities will be required. One of these applications is for load levelling in hybrid electric vehicles and some work has already been undertaken in this area [1,3–8]. Another high-power application is in telecommunications, where short, high power pulses are required [9–11]. This move to higher power will continue and it is desirable to establish some supercapacitor specific testing procedures that will enable a valid comparison between different supercapacitor technologies.

Compared to batteries, supercapacitors can be described as low-energy, high-power, energy storage devices. Supercapacitors are often compared on an energy density basis; however, energy density is not a useful comparison under high-power conditions, as shown below. Power density alone, is also not very informative since it provides no information on the amount of work a supercapacitor can do. Whilst Ragone plots [12] have been used to characterise batteries for many years, supercapacitors have very different characteristics and their behaviour is not always best described using Ragone plots. One noticeable difference is that the power capability of a supercapacitor depends on its state of charge, in contrast to batteries [13]. Another is that supercapacitors may be required to be charged, as well as discharged, at high power. Here we propose power cycling, with the data shown on a Power Cycling Chart (PCC) as an alternative for measuring supercapacitor capability. It combines both energy and power density to provide a tool for clear discrimination between supercapacitors of different characteristics.

* Corresponding author. Tel.: +61-2-9490-8668; fax: +61-2-9490-5311.

E-mail addresses: peter.mahon@cap-xx.com, www.cap-xx.com (P.J. Mahon).

A traditional Ragone plot describes the relationship between energy and power, generally with the assumption of the supercapacitor voltage dropping to half the original voltage (i.e. using three quarters of the energy) and the power delivered into a matched load resistance equal to the Equivalent Series Resistance (ESR) of the supercapacitor. The energy dissipated in the supercapacitor depends on the current and so also on the power level. In some applications, however, the load resistance will change depending on the power required and in many circumstances constant power delivery is required. In our approach, we propose constant power delivery and this is modelled below.

In addition, we will demonstrate that carbon-based supercapacitors have some non-idealities that have a major impact on their high-power performance. The origin of this behavior will be discussed and additional parameters will be described that better characterize the power performance. It will be seen that a constant phase element (CPE) can be substituted for the capacitor in the RC model that is normally used; however, some limitations are still apparent. It is the non-idealities associated with these real devices that are the reasons why we have shied away from the integral equation approach [14–16] at this time.

2. Convolutive modelling of supercapacitor behavior

It is often more convenient to use integral transform methods when dealing with the differential equations encountered in electrical problems and the Laplace transform technique is particularly useful for situations involving convolution integrals. If we consider the response of a resistive circuit element in Laplace space we find that

$$\bar{V}(s) = \bar{I}(s) R \tag{1}$$

for the voltage response resulting from the flow of current through a pure resistor, R, where an overbar indicates the transform of the unbarred quantity and s is the "dummy" Laplace variable. For a pure capacitor, C, it is the link between charge and voltage that is more direct; however, an expression can be written containing the current as long as the current is equal to zero at $t = 0$.

$$\bar{V}(s) = \frac{\bar{Q}(s)}{C} = \frac{\bar{I}(s)}{sC} \tag{2}$$

For a series combination of R and C, the voltages are additive and we can obtain

$$\bar{V}(s) = \bar{I}(s)\left[R + \frac{1}{sC}\right] \tag{3}$$

It is possible to simplify this equation by multiplying it out and Laplace inverting each term separately. However, for reasons that will become apparent later it is convenient to consider the function in brackets as a complicated function of s and therefore it is not possible to find the inverse

Laplace transform of this equation directly. It is possible if the equation is written as

$$\bar{V}(s) = s\bar{I}(s)\left[\frac{R}{s} + \frac{1}{s^2 C}\right] \tag{4}$$

The inverse Laplace transform is

$$V(t) = \frac{\mathrm{d}}{\mathrm{d}t}\left(I(t) * \left[R + \frac{t}{C}\right]\right) \tag{5}$$

and the term in the square brackets is recognizable as the time dependent impedance $Z(t)$ for a simple RC circuit, it follows that

$$V(t) = \frac{\mathrm{d}}{\mathrm{d}t}(I(t) * Z(t)) \tag{6}$$

where the asterisk represents the convolution operation usually represented as a convolution integral and obtained from an inverse Laplace transform

$$f(t) * g(t) = \mathbf{L}^{-1}\{\bar{f}(s)\bar{g}(s)\}$$
$$= \int_0^t f(t - \tau) g(\tau)\mathrm{d}\tau \tag{7}$$

Under constant current conditions, where $I(t) = \Delta I$, Eq. (6) simply devolves into Ohm's law

$$V(t) = \Delta I Z(t) \tag{8}$$

and the voltage response of an RC series circuit to a current step is a voltage step equal to ΔIR superimposed on a linear time ramp with a slope of $\Delta I/C$.

In order to implement the convolution in Eq. (6), we have used an efficient convolution algorithm that has been previously developed which enables the convolute of two functions to be directly calculated [17–19]. That algorithm requires that values of the two functions be known at evenly spaced intervals and the integral of each function or the double integral of one of the functions must be calculable for all times. For the case in which the time dependent functions $I(t)$ and $Z(t)$ are known at time instants of Δ, 2Δ, 3Δ, ..., $L\Delta$, ..., $N\Delta$, where Δ is a brief time interval, N is the total number of points and L is an index such that $I_L = I(L\Delta)$, the convolute can be calculated at each point $t = L\Delta$ from

$$\left[\frac{\mathrm{d}}{\mathrm{d}t}(I(t) * Z(t))\right]_{t=L\Delta}$$
$$= \frac{1}{\Delta}\left[I_L z_1 + \sum_{k=1}^{L-1} I_{L-k}(z_{k-1} - 2z_k + z_{k+1})\right]$$

$$L = 1, 2, \ldots, N \tag{9}$$

The $z(t)$ function is the integral of the $Z(t)$ function with respect to time.

$$z(t) = \int_0^t Z(t)\mathrm{d}t \tag{10}$$

and the integral of $\mathrm{d}I(t)/\mathrm{d}t$ is simply $I(t)$.

It follows that the voltage at any time can be calculated from the current at that time and a straightforward summation using all the previous values of the current. Rearrangement of Eq. (9) also enables the current at a given time to be calculated from the voltage at that instant and the summation term containing all the previously calculated current values

$$I_L = \frac{1}{z_1} \left[V_L \Delta - \sum_{k=1}^{L-1} I_{L-k} (z_{k-1} - 2z_k + z_{k+1}) \right]$$
$$L = 1, 2, \ldots, N \tag{11}$$

The power, $P(t)$, is defined as the product of $V(t)$ and $I(t)$ and it follows that it is possible to substitute for V_L in the algorithm equation to obtain a quadratic equation

$$P_L = \frac{1}{\Delta} \left[I_L^2 z_1 + I_L \sum_{k=1}^{L-1} I_{L-k} (z_{k-1} - 2z_k + z_{k+1}) \right]$$
$$L = 1, 2, \ldots, N \tag{12}$$

This equation can be readily solved to obtain I_L at a given time when the power is known as well as the currents at all the previous times.

3. Supercapacitors, instrumentation and data analysis

The testing methods were applied to two supercapacitors, one was a nominally 8 Farad commercial sample and the other was an 8 Farad model TP249 supercapacitor that we constructed. The model TP249 supercapacitor is based on an activated carbon with an organic electrolyte and it was developed for high-power applications. The Impedance Spectroscopy data was collected using an EG&G PAR273 potentiostat and a Solartron 1250 Frequency Response Analyzer (Solartron Group, Hampshire, England) operating under the control of ZPLOT and analyzed using ZVIEW software (Scribner Associates, Southern Pines, NC, USA). Constant Current and Power Cycling measurements were obtained using a purpose-built power module that was controlled by a computer driven by a Microsoft Visual Basic 6.0 application (Microsoft, Redmond, WA, USA). Cyclic voltammograms were obtained using a BAS 100 A Voltammetric Analyzer with a PWR-3 Power Module (BioAnalytical Systems, West Lafayette, IN, USA). The Constant Current, Power Cycling and Cyclic Voltammetric data were analyzed using non-linear optimization based upon the Marquardt algorithm [20,21] and programmed in Microsoft Visual Basic 6.0.

4. Results and discussion

There are four main methods for the analysis of supercapacitor behavior [22]. They lead to the acquisition of a set of parameters that are considered sufficient to describe the general properties under a wide range of frequency and time domains. We have therefore attempted to characterize two supercapacitors using Impedance Spectroscopy, a Constant Current Charge, Cyclic Voltammetry and constant Power Cycling in order to ascertain whether the results from each method are consistent.

4.1. Impedance spectroscopy

This technique requires relatively sophisticated instrumentation but is by far the most powerful and straightforward method for obtaining the frequency response of a supercapacitor at essentially equilibrium conditions. A small amplitude AC signal is applied at a particular DC bias voltage and the change in magnitude and phase angle relative to the applied AC signal is measured. Figs. 1 and 2 contain plots of the impedance magnitude and phase angle for the TP249 and the commercially available devices as a function of frequency obtained with a DC bias of 0.0 V. The suitability of a series RC model is shown to be insufficient for both cases and an alternative model has been investigated.

The structure of the carbon coating inside the supercapacitor can be considered to be a porous bed of discrete particles held together by a web of binder. The equivalent circuit in this case requires a network of R's and C's to describe each pore and discrete circuit elements are often used [9]. A constant phase element has also been proposed for the mathematical description of porous electrode behavior [1,23–28] and that is the circuit element that we will now consider. It was only when this element was combined in series with R that a significantly improved fit
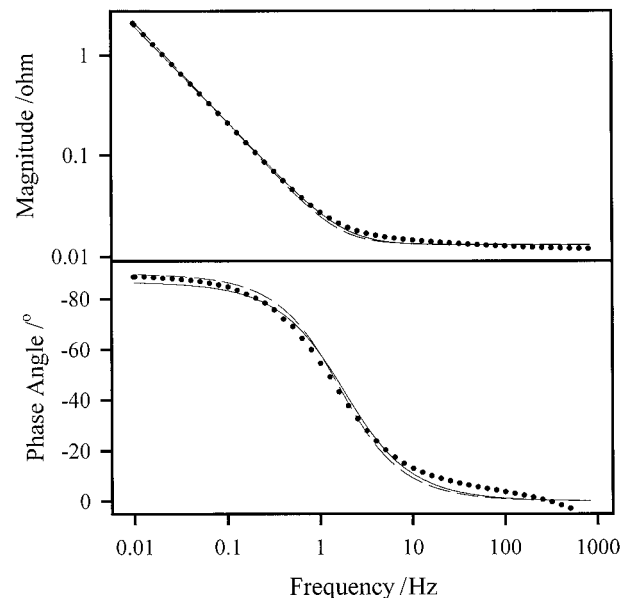

Fig. 1. Impedance Spectroscopy for the TP249 supercapacitor prototype. Solid circles are experimental data, the dashed line is the best fitting RC model and the solid line is from the $RCPE$ model.
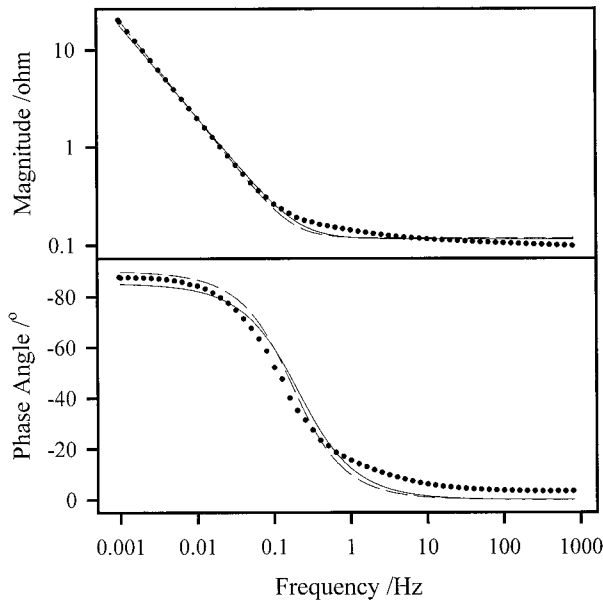
Fig. 2. Impedance Spectroscopy for the commercially available sample. Curves are described in Fig. 1.

was obtained and this is the line that passes closer to the majority of the experimental points in Figs. 1 and 2. Using a CPE, the frequency dependent impedance is described by the equation

$$Z(\omega) = R + \frac{1}{T(i\omega)^p} \tag{13}$$

The resistance term describes the limiting impedance at the high frequency limit and can still be considered to be the ESR of the supercapacitor. The two additional parameters associated with the CPE are the magnitude, T, and the exponent, p, where a straight line in the complex plane plot has an angle of $p\pi/2$. The effect of the CPE is to absorb any inhomogeneity that is not described by the original RC model. This alternate model will be designated as the $RCPE$ model and represents a phenomenological approach whereby the frequency dependent components can be readily converted into the time domain.

Table 1 contains impedance spectroscopy results for the TP249 supercapacitor for both the RC and $RCPE$ models at different DC bias voltages. It can be seen for the RC model that there is a slight voltage dependence for the

parameters. In the $RCPE$ model we observe that the resistance is slightly lower and the T parameter is also lower compared to the capacitance of the RC model. The value of p is approximately 0.96 at the lower voltages and this indicates that the CPE is essentially capacitive.

The corresponding data for the commercially available supercapacitor is given in Table 2. The voltage dependency of the parameters is much more obvious in these results, irrespective of the model used and this appears to be an intrinsic property of this supercapacitor. Interestingly, the resistance decreases by approximately 27% with the increase in voltage but the capacitance increases in a way that compensates so that the apparent time constant ($\tau = RC$) remains relatively voltage independent. The value of T in the $RCPE$ model is significantly less than C in the RC model and p is slightly less at approximately 0.94. The implications of the strong voltage dependence of the parameters for this device will become apparent later when we examine the results obtained from methods that rely on changes in voltage to obtain the parameters.

4.2. Constant current charge

This is the most straightforward of the DC methods and requires the application of a current step to charge or discharge the supercapacitor. It has often been observed that the voltage response for supercapacitors is not ideal and results in some curvature in the measured voltage as a function of time. This effect can be due to a voltage dependent capacitance and/or resistance or possibly due to some other additional time dependent component such as a CPE [28].

The voltage response for an RC circuit was described in Eq. (8); however, the response based on the $RCPE$ model can be obtained from the Laplace inversion of Eq. (13) after substituting "s" in place of "$i\omega$". The time-dependent impedance becomes

$$Z(t) = R + \frac{t^p}{T\Gamma(1+p)} \tag{14}$$

where $\Gamma()$ is the Gamma Factorial function [29]. When combined with Eq. (8), it can be seen that the voltage will be stepped by an amount ΔIR and contain a time-depen-

Table 1
TP249 parameters from Impedance Spectroscopy

Bias voltage (V)	RC		RCPE		
	$R(\Omega)$	$C(F)$	$R(\Omega)$	T	p
0	0.0132	7.41	0.0130	7.32	0.964
0.5	0.0132	7.64	0.0129	7.53	0.964
1	0.0132	7.91	0.0129	7.79	0.961
1.5	0.0135	7.86	0.0131	7.70	0.950
2	0.0142	7.35	0.0136	7.12	0.926

Table 2
Parameters for the commercially available sample from Impedance Spectroscopy

Bias voltage (V)	RC		RCPE		
	$R(\Omega)$	$C(F)$	$R(\Omega)$	T	p
0	0.1181	7.84	0.1150	6.79	0.949
0.5	0.1114	8.15	0.1100	6.93	0.941
1	0.0996	9.45	0.0964	7.97	0.939
1.5	0.0898	10.04	0.0869	8.52	0.942
2	0.0835	10.62	0.0805	8.93	0.939

Table 3
TP249 parameters from Constant Current Charging

Current (A)	RC		RCPE		
	$R(\Omega)$	$C(F)$	$R(\Omega)$	T	p
1	0.0195	10.25	0.0083	8.26	0.930
2	0.0185	9.95	0.0140	8.65	0.940
5	0.0161	9.54	0.0160	8.82	0.941
10	0.0161	9.36	0.0161	9.05	0.939
20	0.0158	9.07	0.0157	9.30	0.926
30	0.0156	9.02	0.0149	10.14	0.872

dent component where p is limited to the range between zero and one.

The results for a variety of current steps under charging conditions are given in Tables 3 and 4 for the two supercapacitors. The data for the *RC* model are obtained from simple analyses where the initial voltage step is divided by ΔI to calculate R and the data from the more linear section of the voltage plot is used to estimate the slope to find C. Reconstruction of the voltage data from the estimated parameters is possible at low currents but becomes less valid as the size of the current step increases and this is demonstrated in Fig. 3 for a 5 A charge of the commercial supercapacitor. Additionally, the estimated value of the capacitance decreases as the size of the current step is increased.

The results from the *RCPE* model for TP249 are reasonably consistent for R but show that T increases and p decreases with an increasing magnitude of the current steps. R and T values are generally higher compared to the impedance spectroscopy results but p is slightly less. The results for the commercial supercapacitor indicates a similar effect for all parameters as observed for TP249, but there is also a more significant trend where p decreases with the magnitude of the current step. It is also apparent that the resistance in this charging case reflects the resistance at zero bias observed in the impedance spectroscopy and T reflects the voltage range accessed during an experiment which is dependent upon the magnitude of the current. *It follows that the model derived in the frequency domain is not really applicable in the time domain for the commercial supercapacitor.* The fact that the model is applicable in both domains for the cap-XX supercapacitor implies that measurement in the frequency domain can be

Table 4
Parameters for the commercially available sample from Constant Current Charging

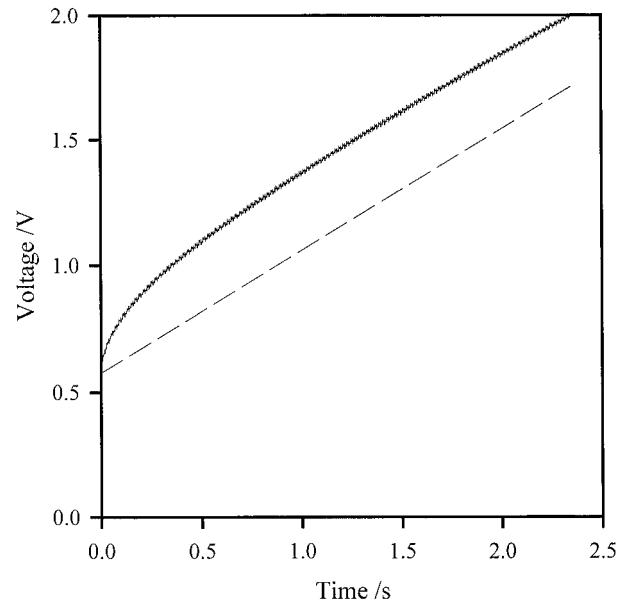| Current (A)	RC		RCPE		
	$R(\Omega)$	$C(F)$	$R(\Omega)$	T	p
1	0.1290	10.91	0.1292	5.77	0.791
2	0.1350	10.71	0.1483	7.01	0.814
5	0.1152	10.34	0.1302	7.60	0.722
10	0.1240	8.76	0.1209	8.46	0.507

Fig. 3. Constant Current Charging data for the commercially available sample. The solid line is the experimental data and the dashed line is the "reconstructed" data from the *RC* model.

used to predict behavior which customers may require in the time domain.

4.3. Cyclic voltammetry

This technique is often used to establish voltage limits but is also important because the measured current is directly relatable to the capacitance in the most straightforward interpretation of the theory.

$$I(t) = C\frac{dV(t)}{dt} \tag{15}$$

However, this equation represents the infinite time or steady state limit and is not obeyed at voltages just after the cycle is commenced and just after the direction of the voltage sweep is changed. For an *RC* circuit, this departure depends on the relative magnitude of the *RC* time constant compared to the time from the start of the experiment and the equation for the forward branch is

$$I(t) = C\frac{dV(t)}{dt}\left[1 - \exp\left(\frac{-t}{RC}\right)\right] \tag{16}$$

For the *RCPE* circuit it is not easy to derive an exact analytical expression but application of the convolution algorithm using Eq. (11) enables the current to be calculated at each voltage. Fig. 4 contains a cyclic voltammogram of the TP249 supercapacitor with a scan rate (i.e. $dV(t)/dt$) of 0.10 V s^{-1} along with the best estimate; once again it is the convolving function that is being adjusted during each iteration of the optimization. The experimental data is plotted at 5 mV intervals for the sake of clarity even though the data density is 1 mV. The
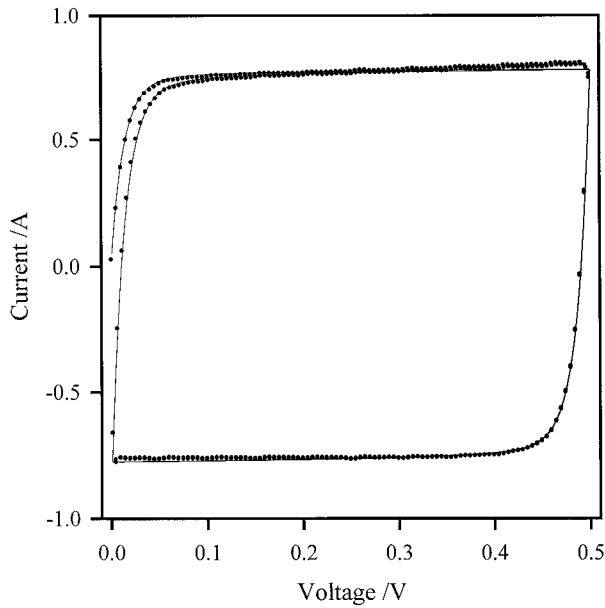
Fig. 4. Cyclic Voltammogram of the TP249 supercapacitor measured at 0.10 V s^{-1}. Solid circles are experimental data plotted at 5 mV intervals for clarity and the solid line is the optimized fit using the *RCPE* model.
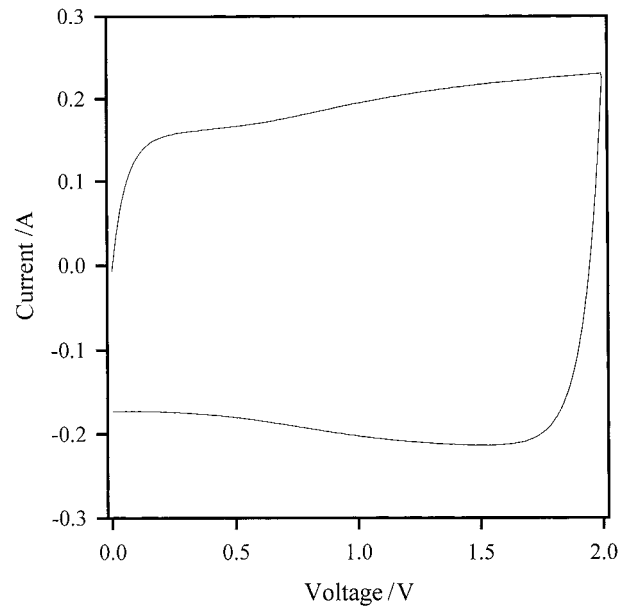

Fig. 5. Cyclic Voltammogram of the commercially available sample measured at 0.02 V s^{-1}.

voltage range was restricted to 0.5 V to ensure that data contained a reasonable region where the time dependence is important and the voltage dependence of the parameters is minimized.

Table 5 contains results derived from the application of non-linear curve fitting using Eq. (11) to various scan rate cyclic voltammograms for the TP249 supercapacitor. The slower scan rates reflect the difficulty of estimating the resistance and this appears to improve as the scan rate increases. The value of T is consistent with the results obtained by the other methods but the value of p is somewhat higher at approximately 0.99. The strong voltage dependence of the parameters is quite apparent for the commercially available supercapacitor as shown in Fig. 5 and the results are not reported because of the large discrepancies.

4.4. Power cycling

Practical measurements of power cycling are relatively straightforward, provided the equipment is available. The procedure is to charge the supercapacitor at the desired power level until the rated or chosen voltage is reached. At this time the polarity of the current is reversed and the supercapacitor then discharges at constant power until the level cannot be sustained or the voltage has decreased to a predefined limit. The polarity of the current is again reversed and the charge cycle is then resumed with cycling between the voltage limits continuing until the measurement is terminated. Fig. 6 contains a typical PCC for the TP249 supercapacitor at 25 W between the voltage limits
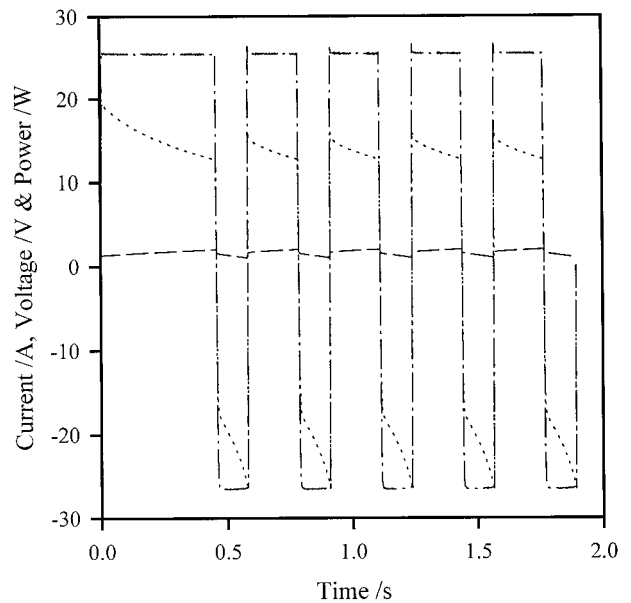

Fig. 6. Power Cycling Chart of the TP249 supercapacitor at 25 W. The dashed line is the voltage (V), the dotted line is the current (A) and the dash-dot line is the power (W).

Table 5
TP249 parameters from Cyclic Voltammetry

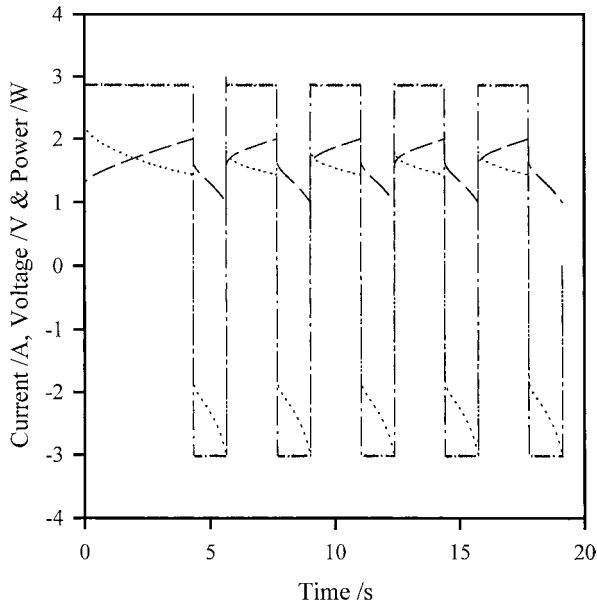| Scan rate (V s^{-1})	RCPE		
	$R(\Omega)$	T	p
0.005	0.0822	7.70	0.990
0.010	0.0304	7.59	0.987
0.020	0.0289	7.70	0.990
0.050	0.0245	7.71	0.991
0.100	0.0191	7.62	0.986

Fig. 7. Power Cycling Chart of the commercially available sample at 3 W. The lines are described in Fig. 6.

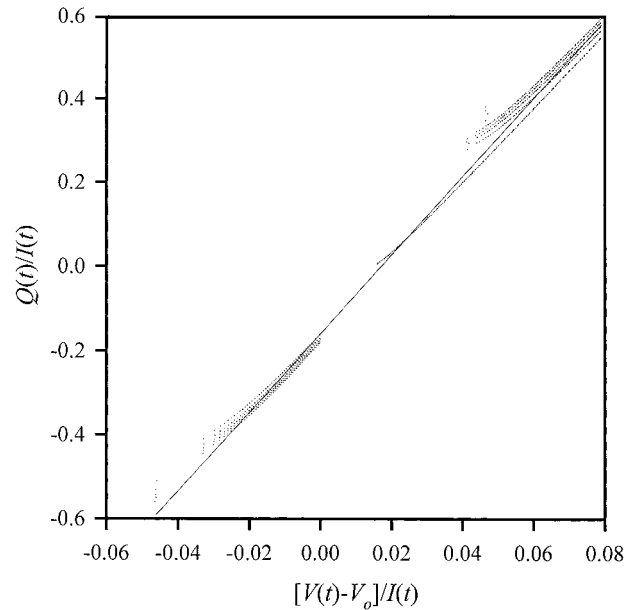Fig. 8. Linear regression analysis of the data from Fig. 6. Solid circles are the experimental data and the solid line is the line of best fit.

of 1.0 and 2.0 V. The effect of increasing the power level is to decrease the ratio of the discharge time to the charge time. The influence of the magnitude of the ESR is to limit the maximum current that can applied to the supercapacitor due to $I(t)R$ losses, resulting in less than expected energy stored during the charge cycle. Eventually all the energy stored is lost during the discharge process to parasitic resistive processes and the theoretical limit for an RC circuit is 0.5 for the ratio of the discharge to the charge cycle.

It is interesting to compare the two supercapacitors with approximately the same relative cycling efficiency. Fig. 7 contains a PCC for the commercially available supercapacitor at 3 W and cycled between the same voltage limits as the TP249 supercapacitor in Fig. 6. It is apparent that much more charge can be cycled through the TP249 supercapacitor because the resistive energy losses are much less at this power level and cycle frequency.

The data for the RC model was calculated from the charge, current and voltage using the following linear regression method. The charge stored in a supercapacitor is

$$Q(t) = C[V_C(t) - V_0] \tag{17}$$

where V_0 is the initial voltage, $V_C(t)$ is the time-dependent voltage across the supercapacitor and is a fraction of the terminal voltage $V(t)$ dependent upon the magnitude of the time-dependent current.

$$V_C(t) = V(t) - I(t)R \tag{18}$$

$Q(t)$ can be evaluated from the integral of the current with respect to time.

$$Q(t) = \int_0^t I(t)\,dt \tag{19}$$

Straightforward substitution of Eq. (18) into Eq. (17) gives

$$Q(t) = C[V(t) - V_0] - I(t)RC \tag{20}$$

Rearrangement produces the linear equation

$$\frac{Q(t)}{I(t)} = C\frac{[V(t) - V_0]}{I(t)} - RC \tag{21}$$

A regression analysis for $Q(t)/I(t)$ versus $[V(t) - V_0]/I(t)$ will have a slope of C and an intercept of RC.

Fig. 8 is a regression plot based on the linearized Eq. (21) for the data contained in Fig. 6 with Figs. 9 and 10
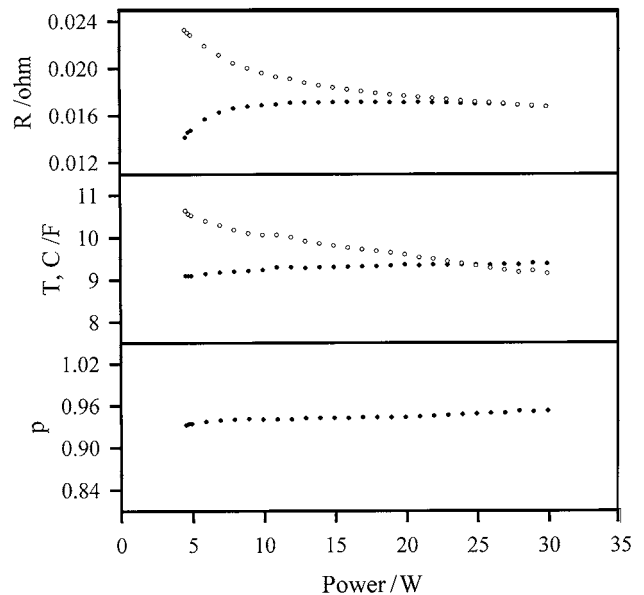

Fig. 9. Results for the RC linearization and non-linear curve fitting using the $RCPE$ model for the TP249 supercapacitor. Open circles are for the RC model and the solid circles are for the $RCPE$ model.

containing the results for power cycling measurements using the two supercapacitors at a range of power levels. The large amount of scatter in Fig. 8 results from an additional time dependent component that can be described by the *RCPE* model. This effect causes the resistance in the *RC* model to be overestimated at low power levels but the estimate improves dramatically as the high-power region is accessed. In the *RC* model the value of *C* is also overestimated at low power levels.

The data for the *RCPE* model is derived from non-linear fitting of the voltage data using the experimental current data and the convolution algorithm given by Eq. (9). In this case it is the convolving function $z(t)$ that is again being modified during each iteration of the optimization process. It is apparent from Fig. 9 for the TP249 supercapacitor that it is difficult to obtain reasonably consistent estimates of the resistance at low power levels; this is due to the relatively small contribution of the resistive term under these low current conditions. The values for the parameters T and p are essentially independent of the power level when plotted on graphs with equivalent axis as the commercially available supercapacitor in Fig. 10.

The data presented in Fig. 10 for the commercially available supercapacitor show that the values from the *RC* model are more consistent as the power is increased. The voltage dependence of the parameters as given in Table 2 show that not only is there a strong voltage dependence but there is also a strong time dependence as described by the CPE. It is the combination of these effects that create the problems demonstrated in Fig. 10 and ensure the difficulty of applying simple models to some supercapacitor technologies.
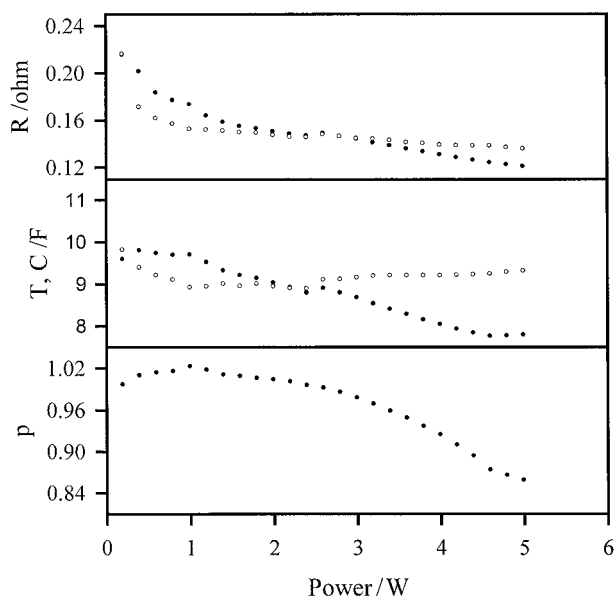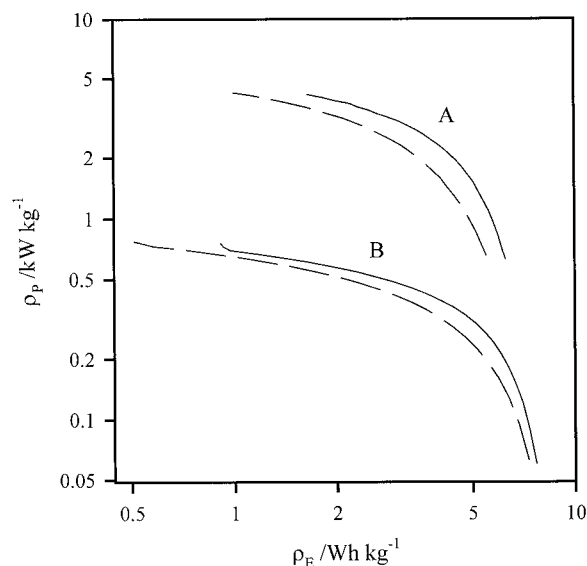

Fig. 11. Ragone plot for both (A) TP249 and (B) commercially available supercapacitors. The solid line is the charge cycle and the dashed line is from the discharge cycle.

The power cycling data is easily converted into a Ragone plot, as shown in Fig. 11. The maximum power level essentially reflects the ESR of each device and it is apparent that the commercially available supercapacitor has already reached its high power limit at comparably low power levels.

5. Conclusion

Predicting performance of supercapacitors in high-power applications is becoming increasingly important. Traditional techniques such as constant current step and impedance measurements, whilst adequately characterizing supercapacitors at low power, do not provide useful information when these characteristics are used to model high-power operation. Supercapacitors utilizing different carbon technology display different behavior during use and the simple *RC* model cannot adequately describe this behavior at any power level.

Constant Power Cycling is proposed as a technique to characterize and distinguish supercapacitors under high-power conditions. The resulting PCC succinctly demonstrates cycle efficiency at desired power levels and can also be used to provide effective simple *RC* values at a chosen power level which can be used to discriminate between different supercapacitor technologies. For the two different supercapacitors examined, *RC* values extracted from constant power measurements were different from Impedance Spectroscopy or Constant Current Charge techniques. For both supercapacitors, the ESR determined from impedance measurements greatly underestimated the apparent ESR under constant power operation. This has

Fig. 10. Results for the *RC* linearization and non-linear curve fitting using the *RCPE* model for the commercially available supercapacitor. Circles are described in Fig. 9.

significant practical implications, such as device efficiency, sizing and capability.

The substitution of a constant phase element for the capacitor significantly improves the modelling of experimental data from impedance and constant current measurements. The *RCPE* model can also be used successfully under constant power conditions, provided that the experimental data quality is adequate and the parameters are independent of voltage.

Acknowledgements

References

[1] B.E. Conway, Electrochemical Supercapacitors: Scientific Principles and Technological Applications, Plenum, New York, NY, 1999.

[2] D.M. Zogbi, in: S. Wolsky, N. Marincic (Eds.), 6th International Seminar on Double Layer Capacitors and Similar Energy Storage Devices, Florida Educational Seminars, Boca Raton, FL,1996.

[3] C.J. Farahmandi, D. Gideon, in: S. Wolsky, N. Marincic (Eds.), 6th International Seminar on Double Layer Capacitors and Similar Energy Storage Devices, Florida Educational Seminars, Boca Raton, FL,1996.

[4] J.R. Miller, in: S. Wolsky, N. Marincic (Eds.), 6th International Seminar on Double Layer Capacitors and Similar Energy Storage Devices, Florida Educational Seminars, Boca Raton, FL,1996.

[5] W.G. Pell, B.E. Conway, W.A. Adams, J. de Oliveira, J. Power Sources 80 (1999) 134.

[6] E. Faggioli, P. Rena, V. Danel, X. Andrieu, R. Mallant, H. Kahlen, J. Power Sources 84 (1999) 261.

[7] G. Gutmann, J. Power Sources 84 (1999) 275.

[8] A.F. Burke, in: S. Wolsky, N. Marincic (Eds.), 9th International Seminar on Double Layer Capacitors and Similar Energy Storage Devices, Florida Educational Seminars, Boca Raton, FL,1999.

[9] J.R. Miller, F.M. Delnick, M. Tomkiewicz (Eds.), Proc. Electrochem. Soc. Symposium on Electrochemical Capacitors 95-29 The Electrochemical Society, Pennington, NJ, 1996, p. 246.

[10] J.R. Miller, in: S. Wolsky, N. Marincic (Eds.), 7th International Seminar on Double Layer Capacitors and Similar Energy Storage Devices, Florida Educational Seminars, Boca Raton, FL,1997.

[11] M.F. Rose, in: S. Wolsky, N. Marincic (Eds.), 8th International Seminar on Double Layer Capacitors and Similar Energy Storage Devices, Florida Educational Seminars, Boca Raton, FL,1998.

[12] D.V. Ragone, Proc. Soc. Automotive Engineers Conference on Rev. of Battery Systems for Electrically Powered Vehicles, Society of Automotive Engineers, Warrendale, PA, 1968.

[13] W.G. Pell, B.E. Conway, J. Power Sources 63 (1996) 255.

[14] V. Srinivasan, C. Lin, J.A. Ritter, J.W. Weidner, in: F.M. Delnick, D. Ingersoll, X. Andrieu, K. Naoi (Eds.), Proc. Electrochem. Soc. Symposium on Electrochemical Capacitors 96-25 The Electrochemical Society, Pennington, NJ, 1997, p. 153.

[15] C.J. Farahmandi, in: F.M. Delnick, D. Ingersoll, X. Andrieu, K. Naoi (Eds.), Proc. Electrochem. Soc. Symposium on Electrochemical Capacitors 96-25 The Electrochemical Society, Pennington, NJ, 1997, p. 167.

[16] V. Srinivasan, J.W. Weidner, J. Electrochem. Soc. 146 (1999) 1650.

[17] K.B. Oldham, Anal. Chem. 58 (1986) 2296.

[18] P.J. Mahon, K.B. Oldham, J. Electroanal. Chem. 445 (1998) 179.

[19] P.J. Mahon, K.B. Oldham, J. Electroanal. Chem. 464 (1999) 1.

[20] D.W. Marquardt, J. Soc. Ind. Appl. Math. 11 (1963) 431.

[21] W.H. Press, S.A. Teukolsky, W.T. Vetterling, B.P. Flannery, Numerical Recipes in FORTRAN: The Art of Scientific Computing, 2nd edn., Cambridge Univ. Press, Cambridge, UK, 1992.

[22] B.E. Conway, W.G. Pell, in: S. Wolsky, N. Marincic (Eds.), 7th International Seminar on Double Layer Capacitors and Similar Energy Storage Devices, Florida Educational Seminars, Boca Raton, FL,1997.

[23] R. de Levie, Electrochim. Acta 8 (1963) 751.

[24] R. de Levie, Electrochim. Acta 9 (1964) 1231.

[25] H. Keiser, K.D. Beccu, M.A. Gutjahr, Electrochim. Acta 21 (1976) 539.

[26] A. Sadkowski, Electrochim. Acta 38 (1993) 2051.

[27] M. Sullivan, R. Kotz, O. Haas, in: F.M. Delnick, M. Tomkiewicz (Eds.), Proc. Electrochem. Soc. Symposium on Electrochemical Capacitors 95-29 The Electrochemical Society, Pennington, NJ, 1996, p. 198.

[28] M. Keddam, H. Takenouti, P. Bernard, S. Senyarich, in: F.M. Delnick, D. Ingersoll, X. Andrieu, K. Naoi (Eds.), Proc. Electrochem. Soc. Symposium on Electrochemical Capacitors 96-25 The Electrochemical Society, Pennington, NJ, 1997, p. 220.

[29] J. Spanier, K.B. Oldham, An Atlas of Functions, Hemisphere, Springer-Verlag, Berlin, 1987.